Centrum voor Wiskunde en Informatica

REPORT*RAPPORT*

MAS

Modelling, Analysis and Simulation

Modelling, Analysis and Simulation

On the dynamics of a mixed parabolic-gradient system

J.K. Krottje

REPORT MAS-R0220 AUGUST 31, 2002

CWI is the National Research Institute for Mathematics and Computer Science. It is sponsored by the Netherlands Organization for Scientific Research (NWO).
CWI is a founding member of ERCIM, the European Research Consortium for Informatics and Mathematics.

CWI's research has a theme-oriented structure and is grouped into four clusters. Listed below are the names of the clusters and in parentheses their acronyms.

Probability, Networks and Algorithms (PNA)

Software Engineering (SEN)

Modelling, Analysis and Simulation (MAS)

Information Systems (INS)

P.O. Box 94079, 1090 GB Amsterdam (NL)
Kruislaan 413, 1098 SJ Amsterdam (NL)
Telephone +31 20 592 9333
Telefax +31 20 592 4199

ISSN 1386-3703

On the Dynamics of a Mixed Parabolic-Gradient System

J.K. Krottje
CWI
P.O. Box 94079, 1090 GB Amsterdam, The Netherlands

j.k.krottje@cwi.nl

ABSTRACT
In the current paper the dynamics of a mixed parabolic-gradient system is examined. The system, which is a coupled system of parabolic equations and gradient equations, acts as a first model for the outgrowth of axons in a developing nervous system. For modeling considerations it is relevant to know the influence of the parameters in the system and the source profiles in the parabolic equations on the dynamics. These subjects are discussed together with an approximation which uses the quasi-steady-state solutions of the parabolic equations instead of the parabolic equations themselves. Some of the findings are demonstrated by numerical simulations.

2000 Mathematics Subject Classification: 70K99, 60J60, 65L05, 92C20.
Keywords and Phrases: parabolic equations, gradient equations, mixed systems, computational neurobiology.
Note: Work carried out under project MAS1.3—Applications from the Life Sciences, continued in 2002 as MAS1.1—PDEs in the Life Sciences.

1 Introduction

In a paper of Hentschel & Van Ooyen [2] a mathematical model is presented on the growth of neural connections in the nervous system. The model describes the outgrowth of axons from neurons to targets in a developmental phase for innervation. It is assumed that the growth toward the targets is partly guided by the concentration gradients of certain chemicals which are present in the environment. These concentration fields change in time due to the release of the chemicals by the targets and the growth cones and the processes of diffusion and absorption.

One of the goals of the model is to better understand the observed effects of bundling and debundling of the growth cones. The assumption that the growth cones themselves, besides the targets, also release chemicals that influence the growth of the cones might explain the bundling and debundling effects.

In the model two kinds of variables are used to describe this phenomenon. First, functions of time $r_\alpha\colon \mathbb{R} \to \mathbb{R}^2$, which denote the positions of the growth cones and where α ranges over the number of axons N_d.[1] Second, fields $\rho_\beta\colon \mathbb{R}^2 \times \mathbb{R} \to \mathbb{R}$, which denote the concentration of the chemicals as a function of space and time, where β ranges over the number of concentration fields N_c. The dynamics are described by gradient equations for the growth cone positions

$$\frac{d}{dt} r_\alpha(t) = \sum_{\beta=1}^{N_c} \lambda_{\alpha,\beta} \nabla \rho_\beta\big(r_\alpha(t), t\big), \tag{1}$$

[1] We will regard the growth cones as 'dynamical sources' to which the subscript 'd' refers.

for all $\alpha = 1, \ldots, N_d$ and for the concentration fields we have parabolic equations

$$\partial_t \rho_\beta(x,t) = D_\beta \triangle \rho_\beta(x,t) - \kappa_\beta \rho_\beta(x,t) + \sum_{\alpha=1}^{N_d} \sigma^d_{\beta,\alpha} S_{r_\alpha(t)}(x) + \sum_{\gamma=1}^{N_s} \sigma^s_{\beta,\gamma} S_{s_\gamma}(x). \tag{2}$$

for all $\beta = 1, \ldots, N_c$. Here $x = (x_1, x_2)$, γ ranges over the number of targets N_s and s_γ denotes the position of target γ.[2] The growth cones and targets act as sources for the concentration fields located at the positions r_α and s_γ. The functions $S_{r_\alpha} : \mathbb{R}^2 \to \mathbb{R}$, where we left out the argument t, can be considered as source profiles for the growth cone sources, which translate with r_α. The coefficient $\sigma^d_{\beta,\alpha}$ can then be interpreted as the excretion strength of growth cone α with respect to chemical β and this coefficient can be a function of time or of the fields $\rho_1, \ldots, \rho_{N_c}$ evaluated at r_α. An analogous interpretation holds for S_{s_γ} and $\sigma^s_{\beta,\gamma}$.

In this paper we want to gain more insight into the dynamics of this mixed system. Although the ultimate goal is to find a suitable numerical method for the system, most of the paper will be analytical work. Verwer and Sommeijer [5] used the explicit Runge-Kutta-Chebyshev method and found that the system is highly sensitive in its parameters and source terms with respect to bundling and debundling. A similar conclusion was reported in a second numerical paper by Lastdrager [3]. Therefore we want to gain understanding on the relative importance of parameters, the sensitivity of the dynamics with respect to these parameters and the effects that the choice of used source functions has on the dynamics, where one can think of block, cone or even δ-functions.

Hentschel & Van Ooyen [2] use in their simulations a quasi-steady-state-approximation (QSSA) for the parabolic equations so that the system reduces to a system of ODEs. By using QSSA, the parabolic equations become elliptic equations that can be solved explicitly in some cases. The solutions then depend on r_α alone and substitution of these solutions in the gradient equations, results in a closed ODE system. We will discuss to what extend QSSA is profitable by examining when it can be used and what its benefits are. As an example we define a specific 1-dimensional system of the form (1)-(2), that we can solve analytically by using the QSSA assumption. We will compare this solution to numerical solutions of the full system.

The contents is as follows. We will start with some remarks on the mixed parabolic-gradient system in Section 2 and the QSSA-approximation in Section 3. In Section 4 we will discuss some possible choices for source functions and in Section 5 we will examine an effect that we will call self interaction. Section 6 is devoted to numerical integration of the system. Here, also, the QSSA solution is compared to the numerical integration of the full system.

2 Mixed Parabolic-Gradient Systems

The system consists of N_d gradient equations (1) and N_c parabolic equations (2). For the domain we will take $t \geq 0$ and $\Omega = [0,1]^2$ and we will assume periodic boundary conditions because the boundary does not play an essential role here and it is convenient from a numerical point of view. Further we need the initial values for r_α and ρ_β. The coupling between the gradient and parabolic equations occurs through the source terms S_{r_α} in the parabolic equations and of course through the gradient terms in the gradient equations.

Gradient equations

We outline some properties of the gradient equations. With the fields ρ_β as given functions of space and time, equation (1) is of the form $\dot{r} = f(r,t)$. If we use the notation $\Phi_\alpha = \sum_\beta \lambda_{\alpha,\beta} \rho_\beta$,

[2] We will regard the targets as 'static sources' to which the subscript 's' refers.

then equation (1) becomes

$$\frac{dr_\alpha}{dt}(t) = \nabla\Phi_\alpha(r_\alpha(t), t). \tag{3}$$

If, for all β, ρ_β is twice continuously differentiable with respect to space and continuous with respect to time, $\nabla\Phi_\alpha$ is Lipschitz continuous and existence and uniqueness of solutions is guaranteed. For a fixed, time independent Φ_α, the stationary points are characterized by $\nabla\Phi_\alpha(x) = 0$. For arbitrary solutions $r(t)$ of (3), $\Phi_\alpha(r(t))$ is nondecreasing in time and therefore, the local maxima of Φ_α are stable stationary points and the minima and saddle points are unstable stationary points of equation (3). The field Φ_α is the weighted sum of the fields $\rho_1, \ldots, \rho_{N_c}$. Hence, r_α tends to grow in a direction of increasing ρ_β with $\lambda_{\alpha,\beta} > 0$ and decreasing ρ_β with $\lambda_{\alpha,\beta} < 0$. The former are called fields of attractants whereas the latter are called fields of repellents.

A point that deserves some attention is that the extrema of Φ_α need not be equal to the maxima and minima (for repellent fields) of the separate ρ_β. This means that if we have a set of targets all contributing to an attractant field, then the stable stationary points of equation (1) need not be equal to the locations of the targets. In particular, if two targets are close to each other, there might be one stationary point in between, instead of two stationary points at the locations of the targets.

Thus far, we have completely ignored the existence of the gradients in the points $(r_\alpha(t), t)$ of the functions Φ_α. We will discuss this in Section 4, where we examine the use of different kinds of source functions.

Parameter ranges and the domain

The parameters values are not known exactly, but we will make assumptions on their orders of magnitude. In the following table some estimated model related quantities are shown.

Parameter	D	v	L_{cones}	L_{target}
Approximate order	$10^{-4}\ mm^2/s$	$10^{-6} - 10^{-4}\ mm/s$	$10^{-6}\ mm$	$10^{-1} - 1\ mm$

Here v is the growth speed of the growing axon, L_{cones} is the diameter of the growth cone and L_{target} is the distance which the axons have to grow across. Further on we will use a parameter ℓ that measures the radius of the (circular) support of the source functions S_{r_α}. It seems reasonable to use $\ell = L_{cones}/2$.

The parameters κ_β, $\sigma^d_{\beta,\alpha}$, $\sigma^s_{\beta,\gamma}$, and $\lambda_{\alpha,\beta}$ are not known and can be used for tuning. However, this does not mean that they can be chosen independently. For instance, the growth speed of axon α at a certain point in time and space is a homogenous function of the parameters $\lambda_{\alpha,1}, \ldots, \lambda_{\alpha,N_c}$ as well as the parameters $\sigma^d_{\beta,\alpha}$ and $\sigma^s_{\beta,\gamma}$ for all α, β and γ. Therefore, if the $\sigma^s_{\beta,\gamma}$ and $\sigma^s_{\beta,\gamma}$ are all multiplied by a certain factor, then the $\lambda_{\alpha,\beta}$ should all be divided by approximately the same factor to keep the speed of the axons in the right range.

All parameters and variables will be measured in units of millimeters and seconds.

3 Quasi-steady-state approximation

We want to consider the use of a quasi-steady-state approximation instead of the parabolic equations (2), as is done in [2]. In this approximation, we use in the gradient equations, not the ρ_β from the parabolic equations, but $\hat{\rho}_\beta$ that are at all times the solutions of the elliptic equations

$$D_\beta \triangle\hat{\rho}_\beta(x) - \kappa_\beta\hat{\rho}_\beta(x) + \sum_{\alpha=1}^{N_d} \sigma^d_{\beta,\alpha} S_{r_\alpha(t)}(x) + \sum_{\gamma=1}^{N_s} \sigma^s_{\beta,\gamma} S_{s_\gamma}(x) = 0, \tag{4}$$

for all $\beta = 1, \ldots, N_c$, given the values of $r_\alpha(t)$. To solve the $\hat{\rho}_\beta$ simultaneously from this system we have to keep in mind that the $\sigma^d_{\beta,\alpha}$ and $\sigma^s_{\beta,\gamma}$ may depend on the $\hat{\rho}_\beta$ evaluated in the points r_α and s_γ.

For instance, the model that is used by Hentschel and Van Ooyen has three fields of chemicals, namely ρ_1 (attractant), ρ_2 (repellent) and ρ_3 (target attractant). Chemicals ρ_1 and ρ_2 are produced by the moving sources and ρ_3 by the static sources and their system of parabolic equations is

$$\begin{aligned}
\partial_t \rho_1(x,t) =& D_1 \triangle \rho_1(x,t) - \kappa_1 \rho_1(x,t) + \sum_{\alpha=1}^{N_d} \sigma^d_{1,\alpha} S_{r_\alpha(t)}(x), \\
\partial_t \rho_2(x,t) =& D_2 \triangle \rho_2(x,t) - \kappa_2 \rho_2(x,t) + \sum_{\alpha=1}^{N_d} \sigma^d_{2,\alpha} \big(\rho_3(r_\alpha(t),t)\big) S_{r_\alpha(t)}(x), \\
\partial_t \rho_3(x,t) =& D_3 \triangle \rho_3(x,t) - \kappa_3 \rho_3(x,t) + \sum_{\gamma=1}^{N_s} \sigma^s_{3,\gamma} S_{s_\gamma}(x),
\end{aligned} \tag{5}$$

where the $\sigma^d_{1,\alpha}$ and $\sigma^s_{3,\gamma}$ are constants. Its steady state, given the values r_α at time t, can be found by setting $\partial\rho_1/\partial t = \partial\rho_2/\partial t = \partial\rho_3/\partial t = 0$ and dropping the arguments t, which results in system (4) for this particular case. Its solution, $(\hat{\rho}_1, \hat{\rho}_2, \hat{\rho}_3)$, is a steady state of system (5) with fixed r_α and when the S_{r_α} and S_{s_γ} are smooth functions or δ-functions (in case of point sources) this state is also globally attracting in the sense that for every set of start functions (ρ_1, ρ_2, ρ_3) the solution of system (5) with fixed r_α tends to $(\hat{\rho}_1, \hat{\rho}_2, \hat{\rho}_3)$ in the L_∞-norm. This is intuitively clear because of the fact that the first and last equation are independent of the equation for ρ_2. Therefore, ρ_1 and ρ_3 approach $\hat{\rho}_1$ and $\hat{\rho}_3$, respectively, so that for $t \to \infty$, the equation for ρ_2 gets constant source terms and ρ_2 converges to $\hat{\rho}_2$.

In general, the coupling between the equations of system (4) by the functions $\sigma^d_{\beta,\alpha}$ and $\sigma^s_{\beta,\gamma}$, might give problems with respect to the existence of steady-state solutions as well as the global attraction of such solutions. We will consider a few different cases illustrating these problems.

Example 1. Concerning the existence of steady-state solutions we look at a simple 1-dimensional example system

$$\begin{aligned}
\partial_t \rho_1(x,t) &= \partial_x^2 \rho_1(x,t) - \rho_1(x,t) + \sigma_1(\rho_1(r_1), \rho_2(r_1))\delta(x - r_1), \\
\partial_t \rho_2(x,t) &= \partial_x^2 \rho_2(x,t) - \rho_2(x,t) + \sigma_2(\rho_2(r_2), \rho_1(r_2))\delta(x - r_2),
\end{aligned} \tag{6}$$

in which the functions ρ_1, ρ_2 are defined on $\mathbb{R}$ and the $\delta(\cdot)$ stand for the Dirac δ-function. If both equations are in steady-state the $\hat{\rho}_1$, $\hat{\rho}_2$ have to satisfy

$$\begin{aligned}
\hat{\rho}_1(x) &= \tfrac{1}{2}\sigma_1(\hat{\rho}_1(r_1), \hat{\rho}_2(r_1))e^{-|x-r_1|}, \\
\hat{\rho}_2(x) &= \tfrac{1}{2}\sigma_2(\hat{\rho}_2(r_2), \hat{\rho}_1(r_2))e^{-|x-r_2|},
\end{aligned} \tag{7}$$

for all $x \in \mathbb{R}$, which follows from the fact that for arbitrary $a > 0$,

$$\left.\begin{aligned} \frac{\partial^2}{\partial x^2}\mu(x) - \mu(x) + a\delta(x) = 0, \quad \forall x \in \mathbb{R} \\ \lim_{x \to \pm\infty} \mu(x) = 0, \end{aligned}\right\} \quad \Longrightarrow \quad \mu(x) = \tfrac{1}{2} a e^{-|x|}.$$

Substitution of r_1 and r_2 in system (7) results in a system of four equations:

$$\begin{aligned}
\hat{\rho}_1(r_1) &= \tfrac{1}{2}\sigma_1(\hat{\rho}_1(r_1), \hat{\rho}_2(r_1)) & \hat{\rho}_1(r_2) &= \tfrac{1}{2}\sigma_1(\hat{\rho}_1(r_1), \hat{\rho}_2(r_1))e^{-|r_2-r_1|} \\
\hat{\rho}_2(r_2) &= \tfrac{1}{2}\sigma_2(\hat{\rho}_2(r_2), \hat{\rho}_1(r_2)) & \hat{\rho}_2(r_1) &= \tfrac{1}{2}\sigma_2(\hat{\rho}_2(r_2), \hat{\rho}_1(r_2))e^{-|r_1-r_2|}
\end{aligned} \tag{8}$$

in four unknowns $\hat{\rho}_i(r_j)$, $(i, j = 1, 2)$. A solution of system (8) will yield a steady-state solution of system (6). However, whether a solution of (8) exists depends on the functions σ_1 and σ_2 and

on the values of r_1 and r_2. For instance, if $\sigma_1(x,y) = \sigma_2(x,y) = xy/((1-x)(1-y))$, then for all choices of r_1 and r_2 the only real solution of system (8) is $\hat{\rho}_1(r_1) = \hat{\rho}_1(r_2) = \hat{\rho}_2(r_1) = \hat{\rho}_2(r_2) = 0$ and therefore the only steady-state of (6) will be $\hat{\rho}_1 \equiv \hat{\rho}_2 \equiv 0$. □

Even if a steady-state solution exists, it can be non-attracting, so that the system will never approach this state. It then doesn't make sense to use the steady-state approximation for solving the gradient equations. An example of such a system is described next.

Example 2. The system of equations is given by

$$\begin{aligned} \partial_t \rho_1(x,t) &= D\partial_x^2 \rho_1(x,t) - \rho_1(x,t) + \sigma_1(\rho_2(r_1))\delta(x-r_1), \\ \partial_t \rho_2(x,t) &= D\partial_x^2 \rho_2(x,t) - \rho_2(x,t) + \sigma_2(\rho_1(r_2))\delta(x-r_2), \end{aligned} \tag{9}$$

with $\rho_{1,2}$ defined on $[0,1]$, periodic boundary conditions, $D = 0.1$, $r_1 = 0.25$, $r_2 = 0.5$ and

$$\sigma_1(x) = \tfrac{1}{2}\frac{x^4}{(\frac{1}{2})^4 + x^4}, \qquad \sigma_2(x) = \tfrac{1}{2}\frac{(1-x)^4}{(\frac{1}{2})^4 + (1-x)^4}. \tag{10}$$

Using the same technique as in Example 1, one can show that system (9) has a steady-state solution. However, numerical experiments show that with the initial condition $\rho_{1,2} \equiv 0$ the system will approach a periodic motion with a period that is around 2. Some pictures of this are shown in Figure 3.1. Thus, system (9) has a steady-state solution which doesn't seem to be an attractor

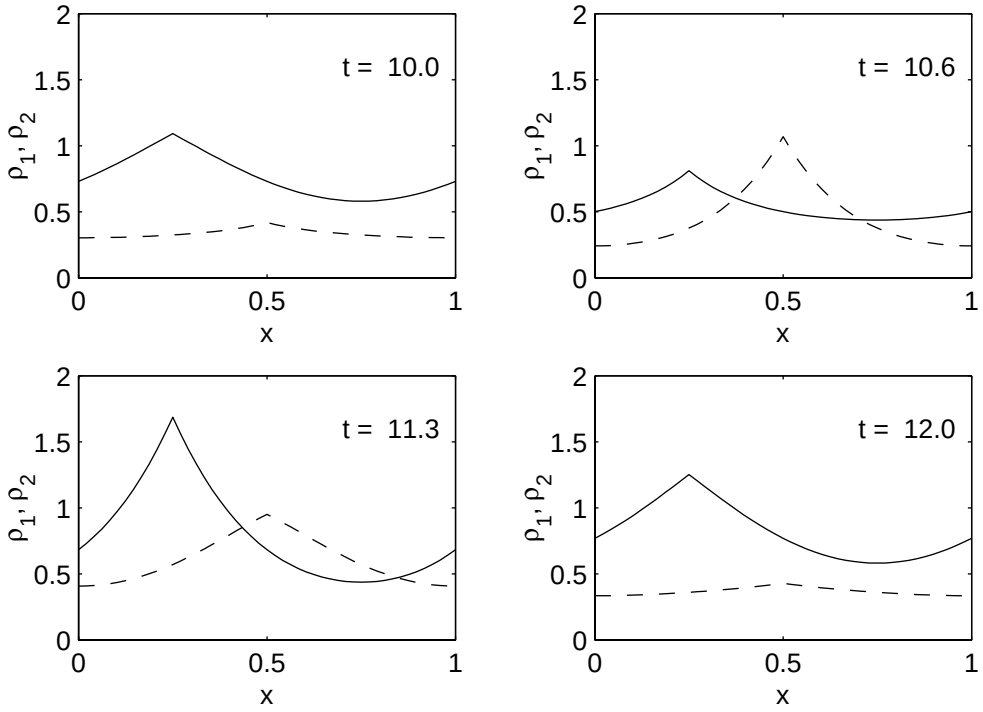

Figure 3.1: Periodic motion of system (9). ρ_1 (—) and ρ_2 (−−).

in the sense that the solution is approached for $t \to \infty$. Therefore, for this system in combination with certain gradient equations no quasi-steady-state approximation can be used. □

In general we can say the following. System (4) can be solved if there is a ordering of the fields ρ_β such that the $\sigma^d_{\beta,\alpha}$ and $\sigma^s_{\beta,\gamma}$ do not depend on $\rho_{\beta_i}(r_\alpha)$ and $\rho_{\beta_i}(s_\gamma)$, for all α and $\beta \le \beta_i \le N_c$.

Solving the system can be done by solving sequentially for $\beta = 1, \ldots, N_c$. We call such a system of equations sequentially dependent. Thus, if the system of parabolic equations is sequentially dependent, then there exists a steady state. In addition, this steady-state is a global attractor of the system.

If, in a mixed parabolic-gradient system, the parabolic equations are sequentially dependent we can use the quasi-steady-state approximation, i.e., the solutions $\hat{\rho}_\beta$ of system (4) can be used in the gradients equations to give

$$\frac{d}{dt} r_\alpha(t) = \sum_{\beta=1}^{N_c} \lambda_{\alpha,\beta} \nabla \hat{\rho}_\beta\big(r_\alpha(t)\big), \tag{11}$$

for $\alpha = 1, \ldots, N_d$. The basic idea behind this approximation is that the dynamics of the parabolic equations is much faster than the dynamics of the gradient equations. However, we will see in Section 5 that with the parameter ranges given in Section 2 this approximation can become very bad in the sense that the growing speeds $\dot{r}_\alpha$ can be significantly retarded if the quasi-steady-state approximation is used.

Another point is what kind of source functions to use. If point sources are being used, the system of elliptic equations (4) can be solved exactly for all arbitrary combinations of $r_1, \ldots, r_{N_d}$, as is done in [2]. We will examine in the next section the use of point sources and different kinds of source functions.

4 Source Functions

We want to consider some aspects of the used source functions S_{r_α} in the parabolic equations. From a modeling point of view, the use of point sources for making the model as simple as possible, is appealing. For instance, Hentschel and Van Ooyen [2] use point sources in their simulations of the model. However, as we will show in the next subsection, using point sources gives difficulties with respect to the smoothness and existence of solutions, especially in 2 and 3 dimensions. The alternative is to use source functions that are spread out in the neighborhood of the source position, as is discussed in Subsection 4.2. Although extra choices have to be made concerning the form of the source functions, the smoothness and existence of solutions are guaranteed in this case.

4.1 Point Sources

We will start with point sources in one dimension, so that we are considering the solutions of equations of the form

$$\partial_t \rho_\beta(x,t) = D_\beta \partial_x^2 \rho_\beta(x,t) - \kappa_\beta \rho_\beta(x,t) + \sum_{\alpha=1}^{N_d} \sigma^d_{\beta,\alpha} \delta(x - r_\alpha(t)) + \sum_{\gamma=1}^{N_s} \sigma^s_{\beta,\gamma} \delta(x - s_\gamma), \tag{12}$$

where $x \in \mathbb{R}$. Because this equation is linear, the solution for given functions $r_\alpha(t)$ can be found by solving the same equation for the different sources separately, meaning that we have to solve equations of the form

$$\partial_t \rho(x,t) = D \partial_x^2 \rho(x,t) - \kappa \rho(x,t) + \sigma \delta(x - r(t)). \tag{13}$$

Smoothness. The solution of equation (13) can be written as

$$\rho(x,t) = \frac{\sigma e^{-\kappa t}}{\sqrt{4\pi D t}} \int_{-\infty}^{\infty} \rho_0(\xi) e^{-\frac{|x-\xi|^2}{4Dt}}\, d\xi + \sigma \int_0^t \frac{e^{-\kappa(t-\tau)}}{\sqrt{4\pi D(t-\tau)}}\, e^{-\frac{|x-r(\tau)|^2}{4D(t-\tau)}}\, d\tau, \tag{14}$$

for all $t > 0$ and $\rho_0(x) = \rho(x, 0)$, which can be easily found by using Fourier analysis. Given $\rho_0 \in L^p$ $(1 \leq p \leq \infty)$, it can be proved that ρ is C^∞ at all points (x, t) with $t > 0$ and $x \neq r(t)$. A proof of this for an analogous equation can be found in [1]. At points $(r(t), t)$, ρ may not be differentiable with respect to x.

Therefore, equation (12) has solutions of ρ_β that are smooth, except in points $(r_\alpha(t), t)$ and (s_γ, t), where the sources are located, as can also be seen in Figure 3.1. For the analogous equations in two and three dimensions the same holds, as can be proved in exactly the same way as in one dimension.

In the complete 1-dimensional mixed parabolic-gradient system, the functions $r(t)$ satisfy gradient equations (1). These equations contain terms $\lambda_{\alpha,\beta}\partial_x\rho_\beta(r_\alpha(t), t)$, so that there can occur something which we will call self-interaction. This occurs if there are α and β with $\sigma^d_{\beta,\alpha} \neq 0$ and $\lambda_{\alpha,\beta} \neq 0$, meaning that source α produces ρ_β and the dynamics of r_α is influenced by ρ_β. In other words, there are sources sensing fields which they help produce themselves.

Ill-definedness. If self-interaction occurs with respect to source α and field β, then the system is not well-defined, because the solution $\rho_\beta(\cdot, t)$ of equation (12) is not differentiable at $r_\alpha(t)$, while the term $\partial_x\rho_\beta(r_\alpha(t), t)$ is used in the gradient equation for $r_\alpha(t)$.

In the 2- and 3-dimensional case the situation is similar. The solution ρ_β is everywhere C^∞, except at the location of the point sources α with $\sigma_{\beta,\alpha} \neq 0$, where it is even singular. Again, this will result in ill-definedness of the problem if self-interaction occurs, in the same way as in the 1-dimensional case. Therefore, if self-interaction occurs, it is impossible to work with point sources.

By defining a generalized gradient $\tilde{\nabla} f(x) = \lim_{h\downarrow 0}(f(x + h) - f(x - h))/(2h)$, we can solve this problem in the 1-dimensional case, because $\tilde{\nabla}\rho_\beta$ exists at the locations of the sources. Further, if f is smooth at x then $\tilde{\nabla} f(x) = \nabla f(x)$. However, it seems that there is not a similar possibility in 2 dimensions due to the fact that the ρ_β are singular at the source locations, which is not the case in 1 dimension. In this case we would like to define a generalized gradient by means of

$$\tilde{\nabla} f(r) = \lim_{h\downarrow 0} \frac{1}{\pi h^3} \int_{B_h(r)} f(x)(x - r)\, dx, \tag{15}$$

with $B_h(r) = \{x \in \mathbb{R}^2 \mid |x - r| = h\}$, for which in case of a smooth function f we can write

$$\begin{aligned}\tilde{\nabla} f(r) &= \lim_{h\downarrow 0} \frac{1}{\pi h^3} \int_{B_h(r)} \Big\{ f(r) + \nabla f(r) \cdot (x - r) + \mathcal{O}\left(h^2\right) \Big\}(x - r)\, dx \\ &= \lim_{h\downarrow 0} \int_{B_h(r)} \frac{1}{\pi h^3} \Big\{ \nabla f(r) \cdot (x - r) \Big\}(x - r)\, dx + \mathcal{O}(h) = \nabla f(r).\end{aligned}$$

However, if we try to use our generalized gradient in two dimensions on a moving source with a constant speed vector $\mathbf{v}$, yielding equation

$$\partial_t\rho(\mathbf{x}, t) = D\triangle\rho(\mathbf{x}, t) - \kappa\rho(\mathbf{x}, t) + \sigma\delta(\mathbf{x} - r(t)), \tag{16}$$

with $r(t) = t\mathbf{v} + r_0$, then for large t the solution approaches

$$\rho(\mathbf{x}, t) = \frac{\sigma}{2\pi D} \exp\left(-\frac{1}{2D}\mathbf{v} \cdot (\mathbf{x} - r(t))\right) K_0\left(\frac{\sqrt{|\mathbf{v}|^2 + 4D\kappa}}{2D}|\mathbf{x} - r(t)|\right). \tag{17}$$

This can be found be substituting a moving profile solution $\rho(\mathbf{x}, t) = \hat{\rho}(\mathbf{x} - t\mathbf{v})$ into equation (16). Here, the function K_0 is the modified Bessel function of the second kind, for which, for small x,

$K_0(x) = -\gamma_E - \ln(x/2) + \mathcal{O}(x)$, where γ_E is Euler's constant. We then can write for $\rho(\mathbf{x}, t)$ in the neighborhood of $r(t)$

$$\begin{aligned}\rho(r+\xi,t) &= \frac{\sigma}{2\pi D}\left\{1 - \frac{1}{2D}\mathbf{v}\cdot\xi + \mathcal{O}\left(|\xi|^2\right)\right\}\left\{-\ln\left(e^{\gamma_E}\frac{\sqrt{|\mathbf{v}|^2+4D\kappa}}{4D}|\xi|\right) + \mathcal{O}\left(|\xi|\right)\right\} \\ &= A_1\ln(A_2|\xi|) + A_3(\mathbf{v}\cdot\xi)\ln(A_2|\xi|) + \mathcal{O}\left(|\xi|\right),\end{aligned}$$

where A_1, A_2 and A_3 are real constants. If this expression is substituted in the definition of $\tilde{\nabla}\rho$, then this yields

$$\frac{1}{\pi h^3}\int_{B_h(0)} \rho(r+\xi,t)\xi\, d\xi = A_3\ln(A_2 h)\mathbf{v} + \mathcal{O}\left(h^0\right),$$

and therefore the limit in the definition of the generalized gradient does not exist at the location of the source $r(t)$. In three dimensions the same effect occurs and again the analogously defined generalized gradient does not exist at the location of the source.

Making use of some kind of generalized gradient doesn't seem to make it possible to combine self-interaction with point sources in the 2- and 3-dimensional case. Because self-interaction is an important feature of the model, we will disregard the use of point sources and concentrate in the next section on sources that are spread-out in space.

4.2 Spread-out sources

If using spread-out sources, certain choices have to be made regarding the form of the source function $S_r\colon \Omega \to \mathbb{R}$. In general, we will define the function S_{r_α} by $S_{r_\alpha}(x) = S(|x - r_\alpha|)$, where $S\colon \mathbb{R}^+ \to \mathbb{R}$. Further we would like to have in most cases a compactly supported source function, meaning that $\mathrm{supp}(S) = [0, \ell]$ for some $\ell > 0$. We assume also that S is non-increasing, piecewise smooth and $\int_\Omega S_{r_\alpha}(\xi)\, d\xi = 1$. In an analogous way we will define S_{s_γ}.

The most simple source function we can think of is the one defined by

$$S(x) = \begin{cases} C_{dim}, & x \le \ell \\ 0, & x > \ell \end{cases}, \qquad C_1 = \tfrac{1}{2\ell}, \quad C_2 = \tfrac{1}{\pi\ell^2}.$$

This function already shows an important feature of spread-out sources. Namely, the source functions S_{r_α} defined using the S above, will have discontinuities at points $x \in \Omega$ with $|x - r_\alpha| = \ell$. This can result in higher order[1] discontinuities at the same points in the solutions ρ_β of the parabolic equations.

Example 3. As an example in one dimension we consider solutions of the equation

$$\partial_t\rho(x,t) = D\partial_x^2\rho(x,t) - \kappa\rho(x,t) + \sigma S(|x - vt|), \tag{18}$$

on $\mathbb{R}$, which describes the dynamics of a concentration field ρ caused by a moving source with location $r(t) = vt$. One of the solutions is a translating profile $\rho(x,t) = \hat{\rho}(x - vt)$, that is shown for $t = 0$ in the left picture of Figure 4.1. At $t = 0$, the source is located at the origin and moves to the right with speed v. Here, we used $v = 0.5$, $D = 0.1$, $\kappa = 1$ and $\ell = 0.5$. In the middle and right picture of the figure $\partial_x\hat{\rho}$ and $\partial_x^2\hat{\rho}$ are shown, respectively. We can see that the second order derivative is discontinuous for $|x| = \ell$. □

In general, solutions of

$$\partial_t\rho(x,t) = D\partial_x^2\rho(x,t) - \kappa\rho(x,t) + f(x,t), \tag{19}$$

[1]With a discontinuity of order r in x we mean that the r^{th}-order derivative is discontinuous in x while the $(r-1)^{\text{th}}$ derivative is continuous. By a discontinuity order of ∞ we mean that all derivatives in x are continuous.

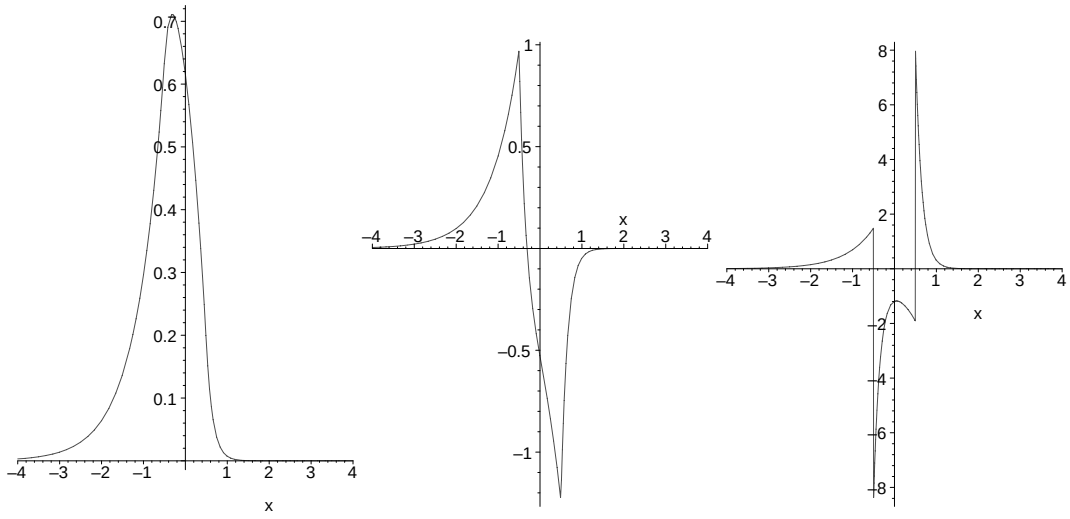

Figure 4.1: Moving source profile $\hat{\rho}$ in one dimension and its derivatives $\partial_x \hat{\rho}$ and $\partial_x^2 \hat{\rho}$.

with $f(x,t)$ piecewise smooth and having discontinuities of order $r_k(t)$ at points $x_k(t)$, are smooth everywhere, except for the points points $x_k(t)$, where they have discontinuities of order $r_k(t)+2$. Therefore we can choose other source functions to guarantee a certain smoothness, some of which are shown Table 4.1.

$S(x)$	C_1	C_2	profile	disc. order of ρ at r	disc. order of ρ at $B(r;\ell)$
C_{dim}	$\frac{2}{\ell}$	$\frac{1}{\pi\ell^2}$		∞	2
$C_{dim}(\ell - x)$	$\frac{1}{\ell^2}$	$\frac{3}{\pi\ell^3}$		3	3
$C_{dim}(x-\ell)^2(x-\frac{1}{2}\ell)$	$\frac{2}{\ell^4}$	$\frac{20}{3\pi\ell^5}$		5	4
$C_{dim}\cos^2(\frac{\pi x}{2\ell})$	$\frac{1}{\ell}$	$\frac{2\pi}{(\pi^2-4)\ell^2}$		∞	4

Table 4.1: Source functions and orders of discontinuity.

Another interesting feature of the moving profile of Example 3 is the fact that its maximum is not attained at the center of the source, although it is very close to it: namely, the maximum is attained in $\mathrm{supp}(S_{r(t)})$, which is equal to $|x - r(t)| < \ell$ in this example. We can prove that this is true for moving profiles in general, by noticing that we must have for $\hat{\rho}$, with $\rho(\mathbf{x},t) = \hat{\rho}(\mathbf{x} - t\mathbf{v})$,

$$D\triangle\hat{\rho}(\mathbf{x}) - \kappa\hat{\rho}(\mathbf{x}) + \mathbf{v}\cdot\nabla\hat{\rho}(\mathbf{x}) = 0, \tag{20}$$

for all $\mathbf{x} \in \Omega\backslash\overline{\mathrm{supp}(S_0)}$, where $\overline{A}$ is the closure of an arbitrary set $A \in \Omega$. If $\hat{\rho}$ would have a maximum at $\mathbf{x} \in \Omega\backslash\overline{\mathrm{supp}(S_0)}$, then $\nabla\hat{\rho}(\mathbf{x}) = 0$ and $\triangle\hat{\rho}(\mathbf{x}) < 0$, because all eigenvalues of the Hessian matrix of $\hat{\rho}$ evaluated in $\mathbf{x}$ are negative and $\triangle\hat{\rho}(\mathbf{x})$ is the sum of these eigenvalues. However, equation (20) yields, by $\hat{\rho}(\mathbf{x}) > 0$ and $\nabla\hat{\rho}(\mathbf{x}) = 0$, that $\triangle\hat{\rho}(\mathbf{x}) > 0$, giving a contradiction. Therefore a maximum of $\hat{\rho}$ lies in $\overline{\mathrm{supp}(S_0)}$ and thus for the maximum of ρ we have that $|\mathbf{x}_{max} - r(t)| \leq \ell$.

5 Self-interaction

It will often occur that the gradient equation of a source contains gradients of one of the fields ρ_β that it produces, which is a property that we called self-interaction in Subsection 4.1. In this section we will see that self-interaction has a diminishing effect on the speeds of the moving sources. Besides this we will examine how the width of the sources influences the self-interaction.

In Example 3, in case of block source functions, the gradient of the field ρ that the source produces, evaluated at the source position, is equal to

$$\partial_x \hat{\rho}(vt) = -\frac{\sigma}{\ell\sqrt{v^2+4D\kappa}} \exp\left(-\frac{\sqrt{v^2+4D\kappa}}{2D}\ell\right) \sinh\left(\frac{v}{2D}\ell\right). \tag{21}$$

The gradient $\partial_x \hat{\rho}(vt)$ is negative (positive), for positive (negative) v, and is decreasing (increasing) with ℓ, as can be proved by noticing that $\sqrt{v^2+4D\kappa}/(2D)$ is always greater than $|v|/(2D)$. This means that for decreasing source width ℓ, the source will sense the fields that it produces in an increasing way. For $\ell \downarrow 0$ this will result in

$$\lim_{\ell \downarrow 0} \partial_x \hat{\rho}(vt) = -\frac{\sigma v}{2D\sqrt{v^2+4D\kappa}}. \tag{22}$$

To get an idea of how big the influence can be on the time derivatives $\dot{r}$ in the gradient equations, we consider an example.

Example 4. In this example we consider a moving source (position r) and a static source (position s) on $\mathbb{R}$, secreting a substance ρ to which the moving source is attracted, yielding equations

$$\partial_t \rho(x,t) = D\partial_x^2 \rho(x,t) - \kappa\rho(x,t) + \sigma S(|x-r(t)|) + \sigma S(|x-s|), \tag{23}$$
$$\dot{r}(t) = \lambda \partial_x \rho(r(t),t). \tag{24}$$

We can write the solution of equation (23) as $\rho(x,t) = \rho_s(x) + \rho_r(x,t)$, where ρ_s and ρ_r satisfy

$$0 = D\partial_x^2 \rho_s(x) - \kappa\rho_s(x) + \sigma S(|x-s|),$$
$$\partial_t \rho_r(x,t) = D\partial_x^2 \rho_r(x,t) - \kappa\rho_r(x,t) + \sigma S(|x-r(t)|),$$

so that for equation (24) we have

$$\dot{r}(t) = \lambda \partial_x \rho_s(r(t)) + \lambda \partial_x \rho_r(r(t),t). \tag{25}$$

In a quasi steady-state approximation the term $\partial_x \rho_r(r(t),t)$ will vanish, however in this case it is approximately equal to the expression in equation (21), which yields after substitution and developing a Taylor series with respect to $\dot{r}$,

$$\dot{r} \approx v + \xi\dot{r} + \eta\dot{r}^3 + \mathcal{O}\left(\dot{r}^4\right), \tag{26}$$

with $v = \lambda\partial_x \rho_s(r)$ and

$$\xi = -\left(\frac{\lambda}{4}\frac{\sigma}{D^2\mu}e^{\mu\ell}\right), \quad \eta = -\left(\frac{\lambda}{96}\frac{\sigma(\mu^2\ell^2+3\mu\ell-3)}{D^4\mu^3}e^{\mu\ell}\right), \quad \mu = \sqrt{\frac{\kappa}{D}}.$$

Solving the approximate equation (26) yields then

$$\dot{r} \approx \frac{1}{1-\xi}v + \frac{\eta}{(1-\xi)^4}v^3 + \mathcal{O}\left(v^4\right). \tag{27}$$

By using parameter values $D = 1.0\cdot10^{-4}$, $\kappa = 1.0\cdot10^{-4}$, $\sigma = 1.0\cdot10^{-3}$, $\ell = 1.0\cdot10^{-2}$, and $\lambda = 1.0\cdot10^{-5}$, where we have that $0 \le v \le 5.0\cdot10^{-5}$, $(1-\xi)^{-1} \approx 0.57$ and $\eta(1-\xi)^{-4} \approx 1.0\cdot10^{6}$, this results in $\dot{r} \approx (0.57)\cdot\lambda\partial_x\rho_s(r)$.

Without self-interaction, as in the case with QSSA, then $\dot{r} = \lambda \partial_x \rho_s(r)$. Hence, according to this estimation, the self-interaction causes a decrease in source speed of 43%. It has to be noted that the quality of this estimation depends on the acceleration of the point source. The used equation (21) is valid for constant $v(=\dot{r})$ and $t \to \infty$ and therefore, if v does not change too rapidly, the convergence of the measured gradient to equation (21) can be faster than the speed with which v changes. □

Self-interaction in two dimensions We next want to examine the effect of the width of source functions on the self interaction in two dimensions. For this, we define $S^\ell \colon \mathbb{R}^2 \to \mathbb{R}$, by $S^\ell(\mathbf{x}) = \frac{1}{\ell^2} S(\frac{1}{\ell}|\mathbf{x}|)$, with $\operatorname{supp} S = [0,1]$, so that

$$\int_{B_\ell(0)} S^\ell(\mathbf{x})\, d\mathbf{x} = \int_{B_1(0)} S(\mathbf{x})\, d\mathbf{x}, \tag{28}$$

where $B_\ell(0) = \{\mathbf{x} \in \mathbb{R}^2 \mid |\mathbf{x}| \leq \ell\}$. Again we consider the moving profile for a source moving with a constant speed $\mathbf{v}$, i.e. $\rho(\mathbf{x}, t) = \hat{\rho}(\mathbf{x} - t\mathbf{v})$. The equation for the field is given by

$$\partial_t \rho(\mathbf{x}, t) = D \triangle \rho(\mathbf{x}, t) - \kappa \rho(\mathbf{x}, t) + \sigma S^\ell(\mathbf{x} - t\mathbf{v}), \tag{29}$$

for which the moving profile will be determined by the equation

$$D \triangle \hat{\rho} + \mathbf{v} \cdot \nabla \hat{\rho} - \kappa \hat{\rho} + \sigma S^\ell = 0, \tag{30}$$

where $\hat{\rho}$ and S^ℓ are functions of $\mathbf{x}$ only. We will solve this equation by using a Green's function $\hat{\rho}_G$, which is the solution of equation (30) with a Dirac distribution δ instead of the function S^ℓ. For these functions we have the expression

$$\hat{\rho}_G(\mathbf{x}) = A_1 e^{(-A_2 \mathbf{v}\cdot\mathbf{x})} K_0\left(A_3|\mathbf{x}|\right) \tag{31}$$

$$A_1 = \frac{\sigma}{2\pi D}, \qquad A_2 = \frac{1}{2D}, \qquad A_3 = \frac{\sqrt{|\mathbf{v}|^2 + 4D\kappa}}{2D} \tag{32}$$

and the solution of equation (30) is then equal to

$$\hat{\rho}(\mathbf{x}) = \int_{\mathbb{R}^2} \hat{\rho}_G(\mathbf{x} - \xi) S^\ell(\xi)\, d\xi. \tag{33}$$

To consider the self interaction, we have to calculate $\nabla \rho(t\mathbf{v}, t) = \nabla \hat{\rho}(0)$. Because of the fact that S^ℓ has support $B_\ell(0)$ and is symmetric at 0, we can write

$$\nabla \hat{\rho}(0) = \int_{B_\ell(0)} \nabla \hat{\rho}_G(\xi) S^\ell(\xi)\, d\xi.$$

The series expansion of $\nabla \hat{\rho}_G$ in the neighbourhood of 0 is equal to

$$\begin{aligned}
\nabla \hat{\rho}_G(\mathbf{x}) =& -\left\{ A_2 A_1 e^{(-A_2 \mathbf{v}\cdot\mathbf{x})} K_0\left(A_3|\mathbf{x}|\right) \right\} \mathbf{v} - \left\{ \frac{A_3}{|\mathbf{x}|} A_1 e^{(-A_2 \mathbf{v}\cdot\mathbf{x})} K_1\left(A_3|\mathbf{x}|\right) \right\} \mathbf{x} \\
=& \left\{ A_1 A_2 \ln\left(e^{\gamma_E} A_3|\mathbf{x}|\right) - A_1 A_2^2 (\mathbf{v}\cdot\mathbf{x}) \ln\left(e^{\gamma_E} A_3|\mathbf{x}|\right) \right\} \mathbf{v} \\
&+ \left\{ -\frac{A_1}{|\mathbf{x}|^2} + A_1 A_2 \frac{\mathbf{v}\cdot\mathbf{x}}{|\mathbf{x}|^2} \right\} \mathbf{x} + \mathcal{O}\left(|\mathbf{x}|\right),
\end{aligned}$$

so that we have for $\nabla \hat{\rho}(0)$,

$$\nabla \hat{\rho}(0) = A_1 A_2 \left(\int_{B_1(0)} \ln\left(e^{\gamma_E + \frac{1}{2}} A_3|\mathbf{x}| \right) S(\mathbf{x})\, d\mathbf{x} + \ln(\ell) \right) \mathbf{v} + \mathcal{O}\left(\ell\right). \tag{34}$$

The effect of self interaction can be estimated by splitting the field ρ into two parts, one part produced by the source ρ_r itself and the other part produced by other sources ρ_e, giving $\mathbf{v}_e = \lambda \nabla \rho_e(r(t), t)$. Using the first term in the equation (34), we can write $\nabla \hat{\rho}(0) = A_4(\ell)\mathbf{v}$. For the speed of the source we then have by the gradient equation $\dot{r} \approx \lambda A_4(\ell)\dot{r} + \mathbf{v}_e$, yielding $\dot{r} \approx (1 - \lambda A_4(\ell))^{-1}\mathbf{v}_e$. With parameter choices of Example 4 we then get $\dot{r} \approx (0.76)\mathbf{v}_e$. Clearly, the self interaction can become infinitely large for small source widths ℓ. The source width is therefore a critical parameter of the system.

6 Numerical Tests

In the previous sections we found by analytic means some properties of the mixed parabolic-gradient systems. In this section we will do some numerical tests to illustrate some of these findings. For this, we use a simple numerical method, which is first order accurate in time and second order accurate in space and serves for showing the effects of self-interaction.

We will concentrate on a 1-dimensional example system (the system from Example 4). The system is

$$\partial_t \rho(x,t) = D\partial_x^2 \rho(x,t) - \kappa\rho(x,t) + \sigma_r S(|x - r(t)|) + \sigma_s S(|x - s|), \tag{35}$$

$$\dot{r}(t) = \lambda \partial_x \rho(r(t), t), \tag{36}$$

which is the most simple system that shows self-interaction. The moving source (position $r(t)$) and the static source (position s) both produce ρ, and the moving source is growing to higher concentrations of ρ. Again, $\operatorname{supp} S = [0, \ell]$, with S of the functions from Table 4.1. Further we will assume that the domain is $[0, 1]$ and we impose periodic boundary conditions.

Numerical Method. For discretization of the parabolic equation (35) we will use the backward-time central-space scheme,

$$\frac{v_m^{n+1} - v_m^n}{k} = D\frac{v_{m+1}^{n+1} - 2v_m^{n+1} + v_{m-1}^{n+1}}{h^2} - \kappa v_m^{n+1} + \sigma_r S(|x_m - r^n|) + \sigma_s S(|x_m - s|) \tag{37}$$

on an evenly spaced grid $0 = x_0, \ldots, x_M = 1$, with gridsize h in space and step size k in time. Because of the periodic boundary conditions we can work with vectors $\mathbf{v}^n = (v_1^n, \ldots, v_M^n)^T$ of length M, such that $v_m^n \approx \rho(x_m, t_n)$. If we denote $S_m(r^n) = \sigma_r S(|x_m - r^n|) + \sigma_s S(|x_m - s|)$, such that $\mathbf{S}(r^n) \in \mathbb{R}^M$, then we can write this scheme as

$$A\mathbf{v}^{n+1} = \mathbf{v}^n + k\mathbf{S}(r^n), \tag{38}$$

where A is a periodic tridiagonal matrix. If we denote the projection of the exact solution $\rho(x,t)$ on the grid by $\boldsymbol{\rho}(t)$, then substitution of this solution into (38) yields

$$A\boldsymbol{\rho}(t_{n+1}) = \boldsymbol{\rho}(t_n) + k\mathbf{S}(r(t_n)) + k\mathcal{O}\left(k + h^2\right), \tag{39}$$

and therefore the discretization is first order consistent in time and second order consistent in space. Further, this scheme is unconditionally stable [4] for a given function $r(t)$.

The path $r(t)$ of the moving source will be approximated at discrete time points t_n ($r^n \approx r(t_n)$). For the discretization of the gradient equation (36), we need to approximate the gradient at r^n, which is not necessarily a grid point x_m. For this, we need a numerical gradient function $P_\nabla : \mathbb{R}^M \times [0,1] \to \mathbb{R}$, such that if an arbitrary, smooth function $f : [0,1] \to \mathbb{R}$ is projected on the grid $\mathbf{x} \in \mathbb{R}^M$, yielding $\mathbf{f} \in \mathbb{R}^M$, then $P_\nabla(\mathbf{f}, r) \approx \partial_x f(r)$. Now we use forward Euler to calculate r^{n+1} from r^n, giving

$$r^{n+1} = r^n + k\lambda P_\nabla(\mathbf{v}^n, r^n). \tag{40}$$

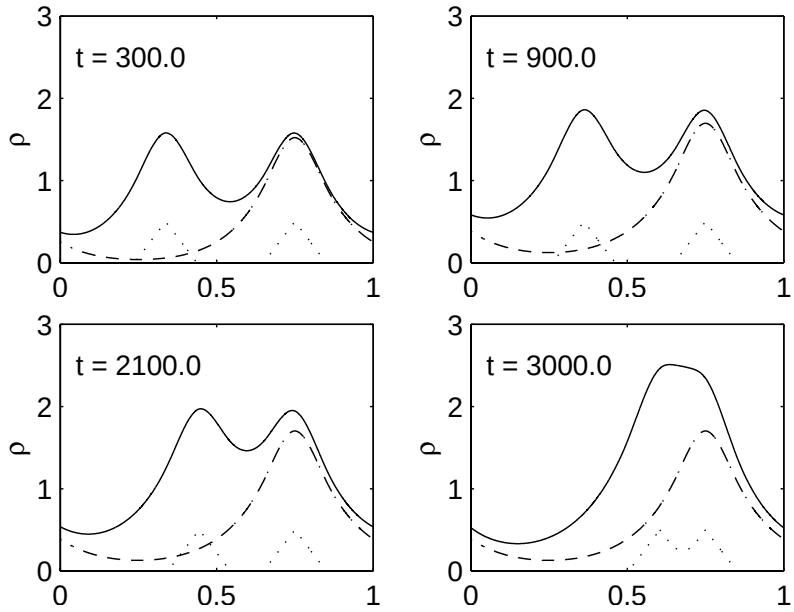

Figure 6.1: Solution of system (35)-(36) at times $t = 300,\ 900,\ 2100,\ 3000$. Sources $(\cdots)$, ρ_s $(- \cdot -)$ and ρ (—).

If we assume that $P_\nabla(\mathbf{f}, r) = \partial_x f(r) + \mathcal{O}(h^p)$ for arbitrary, smooth f, then we can substitute the exact solution $r(t)$ into (40) to obtain

$$r(t_{n+1}) = r(t_n) + k\lambda P_\nabla(\boldsymbol{\rho}(t_n), r(t_n)) + k\mathcal{O}(k + h^p), \tag{41}$$

making scheme (40) first order accurate in time and p^{th} order accurate in space.

Our time stepping process now consists of two stages: equation (38) together with equation (40). But we still need to define the numerical gradient function P_∇. The most straightforward way to define a numerical gradient function is to define

$$P_\nabla(\mathbf{f}, x_i + \theta h) = \tfrac{1}{h}\big(f_{i+1} - f_i\big), \tag{42}$$

with the unique $\theta \in [0,1)$ and x_i such that $r = x_i + \theta h$, which gives $P_\nabla(\mathbf{f}, r) = \partial_x f(r) + \mathcal{O}(h)$, for arbitrary, smooth functions f. However, it is easy to build higher order gradient functions by using more grid points. For example,

$$\begin{aligned} P_\nabla(\mathbf{f}, x_i + \theta h) = \tfrac{1}{h}\Big(&\tfrac{1}{2}\big(-f_{i-1} + 3f_i - 3f_{i+1} + f_{i+2}\big)\theta^2 \\ &+ \big(f_{i-1} - 2f_i + f_{i+1}\big)\theta + \tfrac{1}{6}\big(-2f_{i-1} - 3f_i + 6f_{i+1} - f_{i+1}\big)\Big), \end{aligned} \tag{43}$$

for which $P_\nabla(\mathbf{f}, r) = \partial_x f(r) + \mathcal{O}\left(h^3\right)$ for arbitrary, smooth functions f, which is the highest order numerical gradient function possible using four grid points. We now will show some results of an example calculation using equations (38), (40) and (43).

Example 5. We use the parameter values $D = 1.0 \cdot 10^{-4}$, $\kappa = 1.0 \cdot 10^{-4}$, $\sigma = 3.0 \cdot 10^{-3}$, $\lambda = 1.0 \cdot 10^{-4}$ and the cone-like source functions with $\ell = 0.1$. Further we take $s = 3/4$ and as initial values $r(0) = 1/3$ and $\rho(x, 0) = 0$, for all $x \in [0,1]$ and we will integrate to $t = 3000$. For a calculation with 2000 grid points, both in the x and t-direction ($h = 0.5 \cdot 10^{-3}$ and $k = 1.5$), the results are shown in Figure 6.1. These grid sizes are sufficiently small to approximate exact solutions up to plotting accuracy.

It can be seen that the source at position $r(t)$ moves toward the source at position s. The dash-dotted line shows a ρ-field that is produced solely by the source at s, which we called ρ_s in Example 4. This field isn't used in the calculation, but is shown for illustration purposes. The solid line shows the ρ-field that is used in the calculation. It is the sum of the two fields excreted by the sources. The dotted line displays the scaled source profile functions. They are scaled down by a factor 20 to make them nicely fit into the picture.

In Section 5 we made an estimation of the diminishing effect on the moving speed of a source in case of block source functions and for ρ defined on the whole of $\mathbb{R}$. For our example case, where we have cone source functions and the domain is $[0, 1]$ with periodic boundary conditions, we can do a similar calculation. We then get for ξ in equation (27),

$$\xi = \frac{\lambda\sigma}{4D^2\mu} \frac{(1-\ell)\sinh(\mu\ell) - \ell\sinh(\mu(1-\ell))}{\ell(e^{\mu}-1)(e^{-\mu}-1)}.$$

With our choices of parameters, $\xi = -0.511$ and equation (27) gives $\dot{r} \approx (0.66) \cdot \lambda\partial_x\rho_s(r)$. In the left graph of Figure 6.2 the gradients $\partial_x\rho_s(r(t))$ (dash-dotted line) and $\partial_x\rho(r(t), t)$ (solid line) are shown. Clearly, $\partial_x\rho(r(t), t)$ is much smaller than $\partial_x\rho_s(r(t))$ due to the self-interaction. According to our estimation we should have $\partial_x\rho(r(t), t)/\partial_x\rho_s(r(t)) \approx 0.66$. This ratio is depicted in the right graph. We see that the ratio is a little less than the estimation we made.

Two things might explain this. First, the estimation is based on a moving profile solution moving with constant speed $\dot{r}$. The fact that $\dot{r}$ is not constant, but increasing, might give some differences. Second, from the gradient of the moving profile solution we only take the first order term in $\dot{r}$ in our estimation. For higher speeds, higher order terms can come into play and they then have to be accounted for.

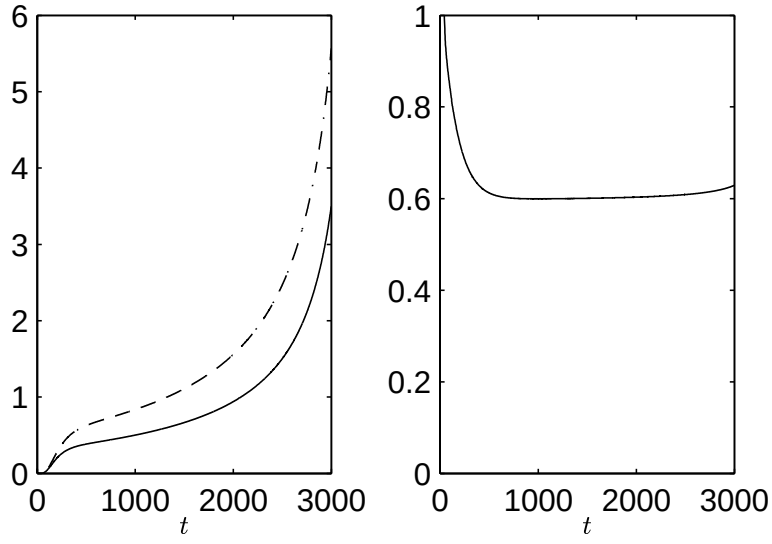

Figure 6.2: Left: $\partial_x\rho(r(t), t)$ (—) and $\partial_x\rho_s(r(t))$ $(-\cdot-)$ against time. Right: ratio of the gradients against time.

We see that the self-interaction causes a decrease of about $30\% - 40\%$ in moving speed of the source here. If QSSA is used the self-interaction is automatically neglected, because concentration fields in steady-state do have a vanishing gradient at the location of the source. Therefore, with QSSA, sources seem to move faster than they really do. In Figure 6.3 the QSSA solution for $r(t)$ (dash-dotted) is shown next to the full integration solution of $r(t)$ just calculated. Clearly, in the QSSA solution the moving source reaches the static source too early.

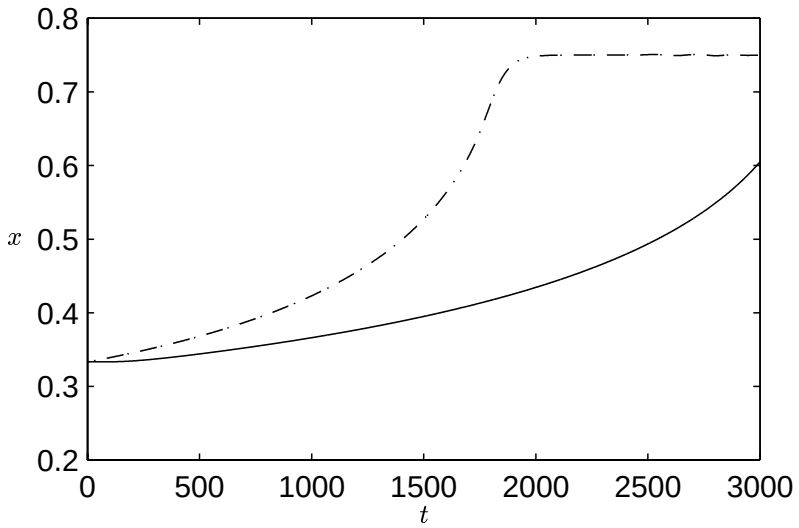

Figure 6.3: Location of the moving source against time computed with QSSA ($- \cdot -$) and with numerical integration of the full parabolic-gradient system (—).

Using QSSA, we turned the parabolic equation into an elliptic equation by putting $\partial_t \rho = 0$. This equation can be solved analytically and its solution, which depends on $r(t)$ can be used in the gradient equation, resulting in an autonomous ODE. We solved this equation numerically using the classical Runge-Kutta 4^{th}-order integration scheme. □

7 Conclusions

In this paper we examined a mixed parabolic-gradient system, which is a prototype for such systems arising in neurobiology, where they act as a model for the axonal growth out of neurons. The long term goal is to develop efficient numerical methods for solving such equation systems. Here, we tried to get a better understanding of the equations by analytical and numerical means.

We found that, with the parameters in the estimated ranges, putting the parabolic equations in steady-state gives very different results. Although some reasons to justify the quasi-steady-state approximation exist, see [2], this approximation can give moving speeds of the sources that are too high, in case self-interaction occurs.

A way to estimate the self-interaction effect is found and by using this, it should be possible to give an indication of the quality of the quasi-steady-state approximation in particular cases. In addition, we found as a rule of thumb, that decreasing the source width will give a greater self-interaction effect. In one dimension this effect seems to be bounded for decreasing source widths, but in two and three dimensions this can become unbounded, resulting in source speeds that are almost zero.

This brings us to the use of point sources. With point sources the solutions of the parabolic equations are smooth everywhere except for the locations of the sources. If self-interaction occurs, gradients have to be taken at these locations, making the combination of self-interaction and point sources impossible. In one dimension we can work around this by redefining the gradients, but in two and three dimensions this seems not to be possible. As an alternative, sources that are spread out in space can be used, but then care has to be taken on the smoothness of solutions of the concentration fields.

In doing the numerical tests we found that the number of grid points needed to reach good accuracy is very high, even for the simple problem we used. In future research we will focus on this aspect and search for better ways to discretize these equations.

Other points of interest are how the model can be extended to make it more realistic. For instance, the model relates certain mechanisms (e.g. sensing gradients) to global behaviour (e.g. bundling). However, the dynamics can be such that at a certain moment of time the mechanisms are not realistic anymore and other mechanisms should take over.

References

[1] Karl E. Gustafson. *Introduction to Partial Differential Equations and Hilbert Space Methods.* John Wiley & Sons, second edition, 1987.

[2] H.G.E. Hentschel and A. van Ooyen. Models of axon guidance and bundling during development. *Proc. R. Soc. Lond. B.*, 266:2231–2238, 1999.

[3] B. Lastdrager. Numerical solution of mixed gradient-diffusion equations modelling axon growth. Technical Report MAS-R0203, Centrum voor Wiskunde en Informatica, P.O. Box 94079, 1090 GB Amsterdam, The Netherlands, January 2002.

[4] John C. Strikwerda. *Finite Difference Schemes and Partial Differential Equations.* Chapman & Hall, 1989.

[5] J.G. Verwer and B.P. Sommeijer. A numerical study of mixed parabolic-gradient systems. *J. Comp. Appl. Math.*, 132:191–210, 2001.